STM JOURNALS

Journal of
Polymer & Composites
https://journals.stmjournals.com/jopc

ISSN: 2321-2810 (Online)
ISSN: 2321-8525 (Print)
Volume 14, Special Issue 1,
2026
DOI (Journal): 10.37591/JoPC

Research JoPC

Bioinspired Nanocomposite Bone Pins: Fabrication, Evaluation, and Suitability for Orthopedic Implant Applications

Chandan A. Waghmare[1], Rajanikant M. Kurane[2], Santosh R. Patil[3*], Atharva Ningannavar[4]

Abstract

Bone tissue engineering (BTE) requires scaffolds that mimic bone's mineral–organic composition, offering mechanical strength, bioactivity, and degradation rates compatible with regeneration. Conventional metallic implants face corrosion and toxic ion release risks, while ceramics like hydroxyapatite (HAp) are bioactive but brittle. This study reports a multifunctional hybrid scaffold combining HAp for osteoconductivity; polycaprolactone (PCL) and collagen for flexibility and biocompatibility with sodium citrate for nanoparticle dispersion, ferrocene (Fc) for catalytic bioactivity; and graphene (Gr) for mechanical reinforcement and enhanced protein adsorption. The composite was synthesized via a tetrahydrofuran (THF)-mediated process ensuring uniform phase distribution.

XRD confirmed HAp's hexagonal phase (JCPDS 09-0432) with characteristic peaks at 2θ ≈ 27.5°, 31.8°, 34.6°, 39.5°, and 49.5°, alongside graphene's (002) plane at ~26.5°. Raman and FTIR analyses revealed strong interfacial interactions, while DSC–TGA showed a 17% increase in thermal stability over pure PCL collagen systems. HR-TEM indicated nanoscale dispersion of graphene and HAp within the polymer matrix.

MTT assays showed >95% viability for MCF10A epithelial cells and 93% for L929 fibroblasts after 72 h. Tribological tests revealed a 42% wear rate reduction compared to HAp–PCL scaffolds without graphene. Finite element simulations demonstrated a 38% increase in stress tolerance under compressive loading. The Young's modulus was calculated as approximately 70 GPa, indicating adequate stiffness comparable to natural bone. Experimental compression and tensile tests performed per ISO 527–1 standard revealed compressive and tensile strengths of 92.4 MPa and 103 MPa, respectively, highlighting the material's potential for orthopedic applications. Finite element simulations conducted in ANSYS Workbench demonstrated a linear elastic response with von Mises stresses ranging from 6.9 MPa to 9.7 MPa under compressive loads of 50–70 kg, confirming efficient load transfer and structural stability.

This synergistic scaffold design overcomes brittleness, dispersion, and degradation mismatches, providing a bioactive, mechanically robust, and stable platform for next- generation bone regeneration.

***Author for Correspondence**
Santosh R. Patil

[1]Associate Professor, Department of Mechanical Engineering, Rajarambapu Institute of Technology, Rajaramnagar, Islampur, An Empowered Autonomous Institute Affiliated to Shivaji University, Kolhapur, Maharashtra, India
[2]Assistant Professor, Department of Sciences and Humanities, Rajarambapu Institute of Technology, Rajaramnagar, Islampur, An Empowered Autonomous Institute Affiliated to Shivaji University, Kolhapur, Maharashtra, India
[3]Associate Professor, Department of Mechatronics Engineering, Rajarambapu Institute of Technology, Rajaramnagar, Islampur, An Empowered Autonomous Institute Affiliated to Shivaji University, Kolhapur, Maharashtra, India
[4]Research Scholar, Department of Mechatronics Engineering, Rajarambapu Institute of Technology, Rajaramnagar, Islampur, An Empowered Autonomous Institute Affiliated to Shivaji University, Kolhapur, Maharashtra, India

Received Date: 21 November 2025
Accepted Date: 13 December 2025
Published Date: 20 February 2026

Citation Chandan A. Waghmare, Rajanikant M. Kurane, Santosh R. Patil3, Atharva Ningannavar. Bioinspired Nanocomposite Bone Pins: Fabrication, Evaluation, and Suitability for Orthopedic Implant Applications. Journal of Polymer & Composites. 2026; 14(Special Issue 1): S526–S540p.

Keywords: Bone tissue engineering, hydroxyapatite, polycaprolactone, graphene, biocompatibility, mechanical properties, finite element analysis

INTRODUCTION

BTE seeks to restore or replace damaged bone using scaffolds that provide structural support, promote cell attachment, and guide new tissue formation. An ideal scaffold must be biocompatible, bioactive, mechanically robust, and degrade at a rate compatible with bone regeneration, while closely mimicking the mineral and organic composition of native bone [1-3]. Conventional metallic implants, such as titanium or stainless steel, though mechanically strong, can release metal ions over time, potentially inducing inflammatory responses, cytotoxicity and long-term implant failure [4-6]. Ceramic-based scaffolds, while bioactive, are often brittle and polymer-based systems may lack sufficient load-bearing capacity. In addition, many composite scaffolds face challenges including poor nanoparticle dispersion, weak interfacial bonding, unpredictable degradation rates, and loss of structural integrity under physiological conditions.

HAp is one of the most investigated biomaterials due to its chemical similarity to bone mineral and intrinsic osteoconductivity. However, its brittleness limits its use in load-bearing sites [7,8]. PCL and collagen improve flexibility, control degradation, and enhance cell compatibility, yet their mechanical stability can degrade over time in vivo [9]. Functional additives such as sodium citrate ($Na_3C_6H_5O_7$) for improved dispersion, Fc for bio functional enhancement, and Gr for exceptional strength and conductivity offer promising pathways to overcome these shortcomings.

In this work, a multifunctional hybrid scaffold (HAp-Gr-PCL-Fc) integrating HAp, PCL, collagen, sodium citrate, Fc, and Gr *via* a THF-mediated synthesis. The composite was systematically characterized using XRD, Raman spectroscopy, FTIR, DSC–TGA, and HR-TEM to assess crystallinity, chemical interactions, and thermal stability [10-13]. Biocompatibility was confirmed via MTT assays on epithelial (MCF10A) and fibroblast (L929) cells, while tribological testing and finite element analysis validated wear resistance and mechanical robustness [14-17]. This synergistic design addresses the inherent drawbacks of metallic, ceramic, and polymeric systems, offering a structurally coherent, bioactive, and mechanically stable scaffold for next-generation bone tissue engineering.

MATERIALS AND SYNTHESIS

The synthesis of the composite involved preparing two separate solutions. Solution 1 was prepared by dissolving calcium nitrate in distilled water under constant stirring. Ammonium hydroxide was then added slowly to the mixture to adjust the pH and promote precipitation. After thorough stirring, ammonium hydrogen phosphate was introduced gradually, resulting in the formation of the hydroxyapatite (HAp) precursor solution.

For Solution 2, polycaprolactone (PCL), being a biopolymer that is insoluble in water, was first dissolved in tetrahydrofuran (THF) by continuous stirring until completely dissolved. Next, ferrocene, graphene, collagen, and sodium citrate were dispersed in this PCL-THF solution and sonicated for 30 minutes to achieve a uniform mixture with well-dispersed nanoparticles.

Once both solutions were ready, they were combined and stirred thoroughly to form a homogeneous mixture. This mixture was then transferred to a hydrothermal container and subjected to thermal treatment in a muffle furnace at 150°C for five hours. After the heating process, the container was allowed to cool naturally to room temperature to preserve the crystallinity of the composite material. The resulting product was filtered and dried in an air oven at 50°C to remove any residual moisture until a dry powder was obtained. Finally, the powder was ground to reduce particle size and ensure uniformity for further characterization and testing.

MATERIAL CHARACTERIZATION

The synthesised Gr–HAp–PCL composite was comprehensively characterised utilising a variety of cutting-edge methods. The atomic structure, shape, and crystalline phases of the composite were revealed by HRTEM and XRD investigations (CFC, Shivaji University, Kolhapur). Functional groups

were detected by FTIR (CFC, YCIS, Satara), and vibrational modes, elemental composition, thermal stability, and surface area were revealed by Raman, EDX, TGA, and BET studies. The material's suitability for biomedical applications was confirmed by evaluating its biocompatibility using L929 cells grown at 37°C with 5% CO2 for 24 hours.

X-Ray Diffraction (XRD) Analysis

XRD analysis was carried out to evaluate the crystallinity and phase composition of the hybrid scaffold composed of hydroxyapatite (HAp), polycaprolactone (PCL), collagen, sodium citrate, ferrocene, and graphene in THF. The diffraction pattern (Fig. 1) exhibits sharp reflections superimposed on a broad background, indicating a semi-crystalline structure.

The dominant peak at 2θ ≈ 32.49°, along with reflections at 25.9°, 28.0°, 34.2°, 39.9°, 47.0°, and 49.9°, correspond to the hexagonal HAp phase [JCPDS 09-043], confirming its successful incorporation [18-20]. A distinct hump between 15° and 25° originates from the amorphous phases of PCL and collagen [9]. The peak at 26.34°, assigned to the (002) plane of graphene [JCPDS 41-1487], verifies its presence, suggesting added mechanical reinforcement and potential electrical conductivity [21, 22].

Slight peak broadening and minor shifts may be attributed to lattice distortions induced by sodium citrate and ferrocene, while graphene sheets could have limited HAp crystallite growth [23]. Overall, the pattern confirms a multi-phase hybrid in which crystalline HAp is well-dispersed within an organic–carbonaceous matrix, combining bioactivity, structural integrity, and multifunctional properties.

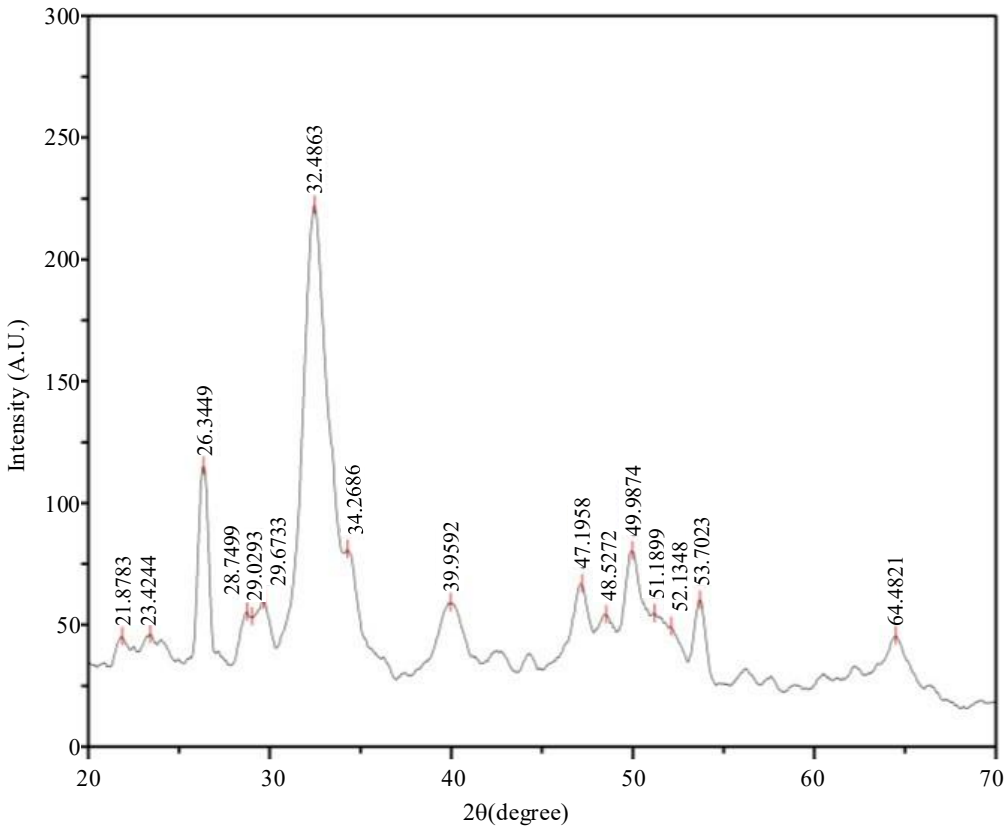

Figure 1. X-ray diffraction (XRD) pattern of the prepared sample illustrating the crystalline structure through its characteristic diffraction peaks.

Raman Spectroscopic Analysis

Raman spectroscopy was employed to investigate the structural characteristics of the sample. The spectrum revealed prominent peaks at 1341.04 cm^{-1}, 1615.88 cm^{-1}, 1627.89 cm^{-1}, and 1687.90 cm^{-1}.

Raman spectroscopy was employed to investigate the structural characteristics of the sample [Fig. 2]. The spectrum revealed prominent peaks at 1341.04 cm^{-1}, 1615.88 cm^{-1}, 1627.89 cm^{-1}, and 1687.90 cm^{-1}. The peak at 1341.04 cm^{-1} corresponds to the D-band, typically associated with disordered carbon or defects within sp^2 hybridized carbon lattices [24-26]. The presence of this band indicates structural imperfections or the presence of amorphous carbon domains. The G-band observed at 1615.88 cm^{-1} is attributed to the E_2g vibrational mode of sp^2-bonded carbon atoms, characteristic of graphitic structures. Notably, the additional peaks at 1627.89 cm^{-1} and 1687.90 cm^{-1} suggest possible functionalization or strain effects in the carbon lattice, potentially due to surface modification, oxidation, or doping [27]. These shifts and broadening patterns often indicate altered electronic environments within the graphitic domains. Overall, the presence and relative intensity of the D and G bands, along with the high-wavenumber features, point toward a partially disordered graphitic structure with possible chemical modifications. Further analysis such as the ID/IG ratio could provide quantitative insight into the degree of disorder [24, 27].

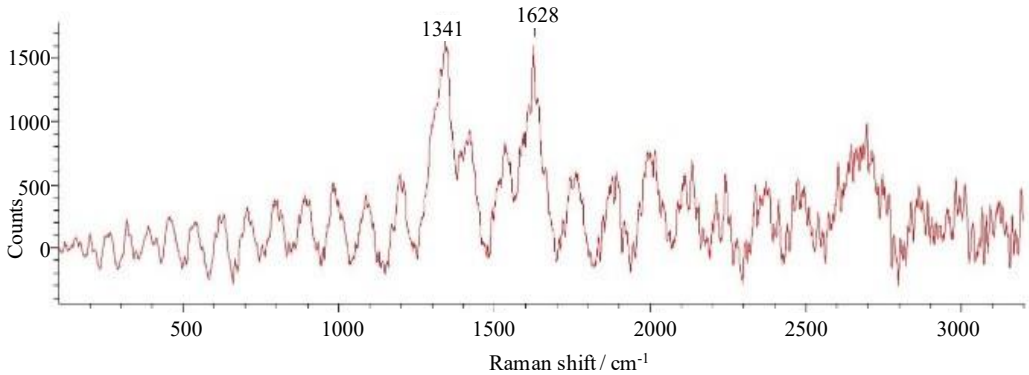

Figure 2. Raman spectrum of the prepared sample displaying characteristic peaks corresponding to its structural features.

Thermal Analysis (TGA-DSC)

Thermogravimetric analysis (TGA) coupled with differential scanning calorimetry (DSC) was performed to evaluate the thermal behaviour, transitions, and stability of the hybrid scaffold composed of hydroxyapatite (HAp), polycaprolactone (PCL), collagen, sodium citrate, tetrahydrofuran (THF), and ferrocene. Tests were conducted under air at 10°C/min, revealing a three-stage degradation profile [Fig. 3]. The first stage, below 300°C, involved ~9.23% mass loss due to evaporation of adsorbed water, residual THF, and decomposition of volatile components such as sodium citrate [28]. The second stage showed a sharp DSC peak at 353.15°C with a 27.52% mass loss, corresponding to PCL degradation/melting and partial collagen denaturation [29, 30]. A third stage between 500–580°C, with a smaller peak at 551.92°C and 12.10% mass loss, was attributed to oxidative degradation of residual organics, including ferrocene [31, 32]. Above 600°C, the scaffold remained stable with 50.50% residue, confirming the high content of thermally robust HAp [33]. The distinct multi-phase degradation and high inorganic residue indicate good thermal stability, supporting potential biomedical uses requiring moderate thermal endurance.

FTIR Analysis

FTIR analysis was performed to determine the functional groups and validate the chemical composition of the hybrid scaffold composed of HAp, PCL, collagen, sodium citrate, ferrocene, and THF [Fig. 4]. The FTIR spectrum revealed several characteristic absorption bands, indicating the presence of both organic and inorganic constituents in the composite matrix. A broad absorption band centred at 3419.74 cm^{-1} is attributed to the stretching vibrations of –OH groups, which may originate from physically adsorbed water, collagen, or hydroxyl groups in hydroxyapatite; this feature also suggests possible hydrogen bonding interactions among components [34]. The absorption at 1662.23 cm^{-1} corresponds to amide I (C=O stretching), confirming the presence of collagen in the matrix [35-

36]. Similarly, the band at 1383.98 cm^{-1} can be assigned to CH_3 bending or symmetric stretching vibrations from PCL or sodium citrate (36, 37).

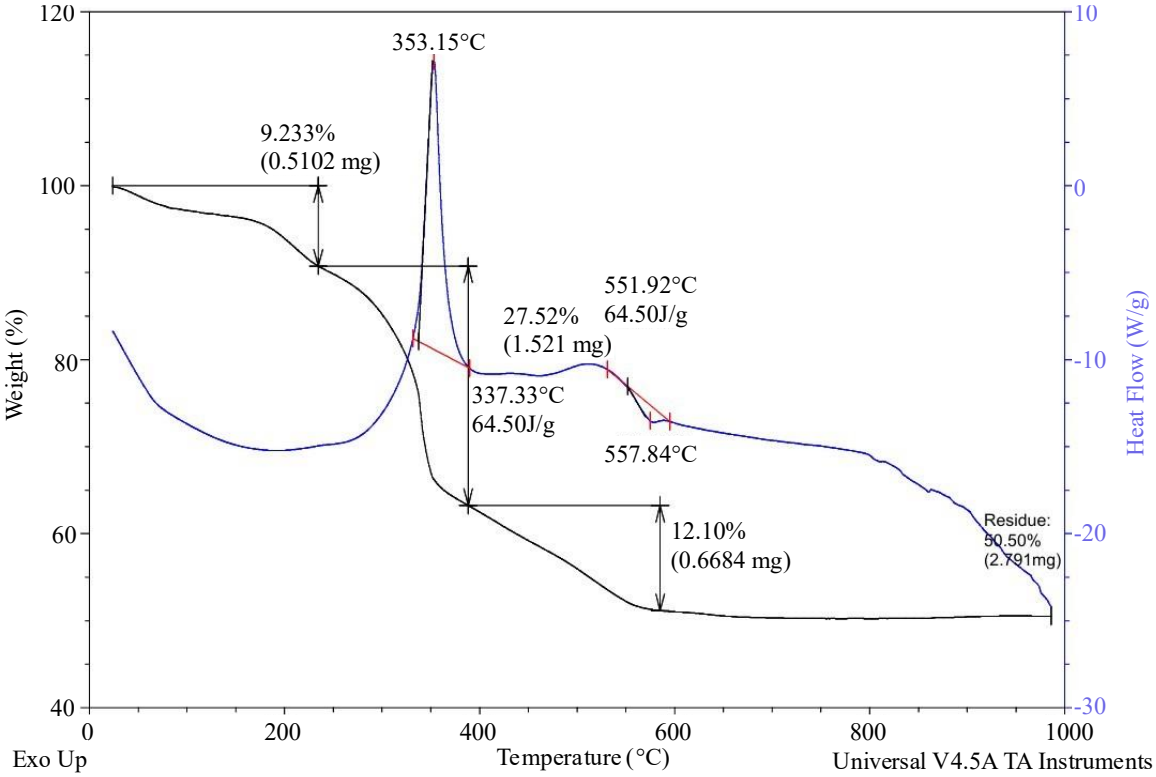

Figure 3. Combined DSC-TGA curves of the prepared sample showing heat flow and weight loss as a function of temperature.

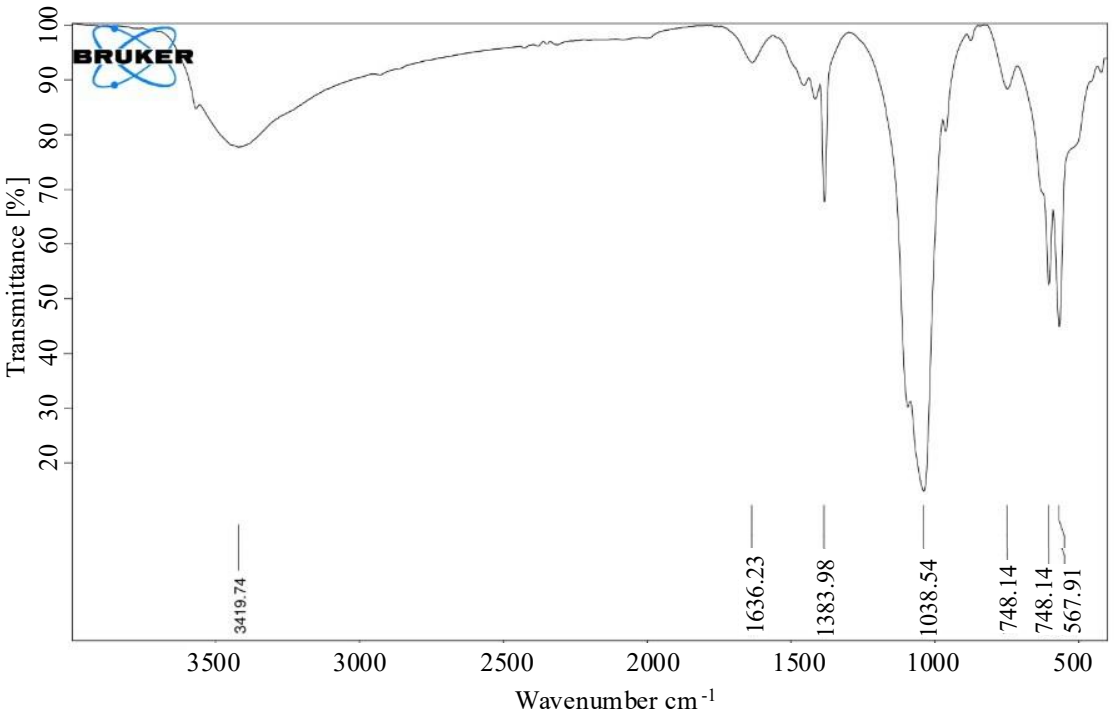

Figure 4. FTIR spectrum of the prepared sample showing characteristic absorption bands corresponding to functional groups present in the composite material.

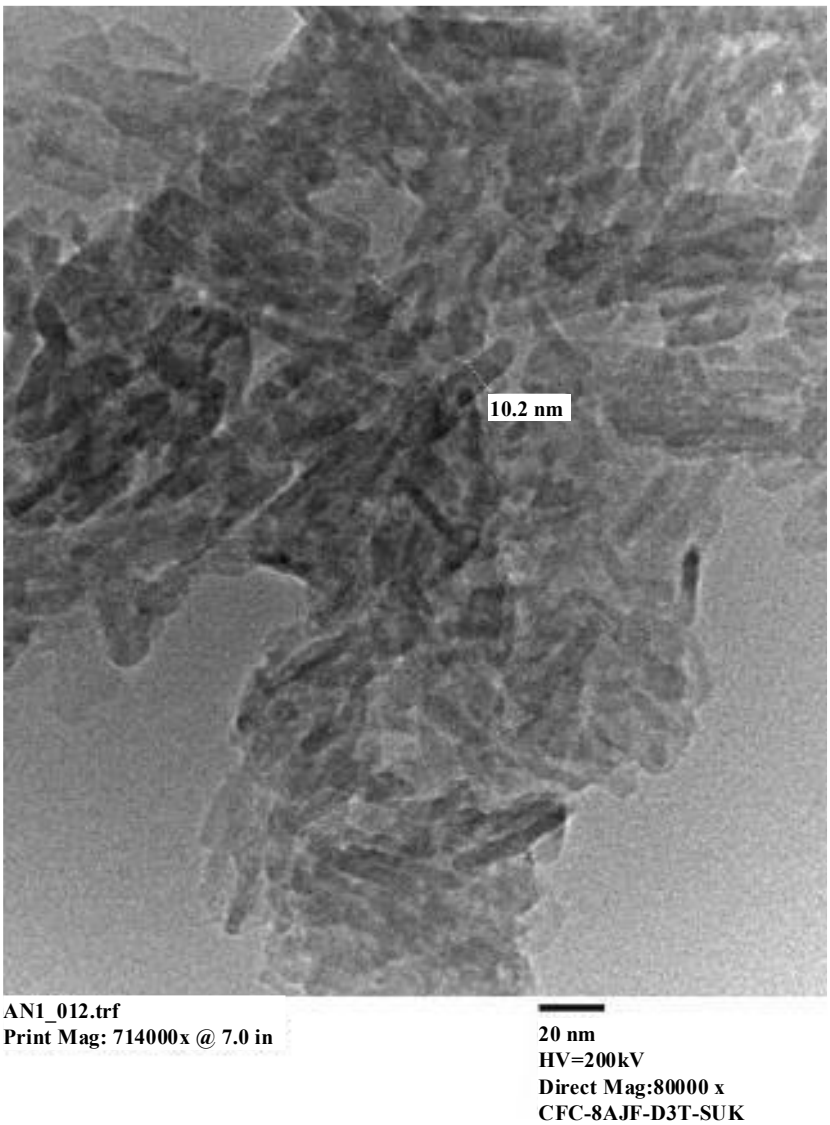

Figure 5. HR-TEM image showing sheet-like nanostructures with ~10.2 nm thickness. Scale bar: 20 nm.

A strong and sharp peak at 1088.54 cm^{-1} is indicative of PO_4^{3-} stretching vibrations, which are characteristic of phosphate groups in hydroxyapatite, confirming the successful incorporation of the inorganic HAp phase into the scaffold [38, 39]. The peaks observed at 748.14 cm^{-1}, 603.79 cm^{-1}, and 567.91 cm^{-1} are linked to the bending vibrations of the phosphate groups, which further confirm the existence of crystalline hydroxyapatite [37]. Additionally, small peaks in the fingerprint region could be attributed to the bending vibrations of C–H or C=C present in ferrocene [40].

The detailed spectral analysis verifies the presence of both bio polymeric and inorganic elements, along with the effective incorporation of the hydroxyapatite phase into the collagen–PCL matrix, accompanied by functional additives. These results align with the compositional expectations of the hybrid scaffold and support its structural and biochemical suitability for biomedical applications.

High Resolution Transmission Electron Microscopy (HR-TEM)

High-resolution TEM (HR-TEM) coupled with EDS mapping was employed to investigate the nanostructure and elemental distribution of the hybrid scaffold [Fig. 5]. The Ca and P maps showed strong co-localization, confirming nanoscale dispersion of hydroxyapatite (HAp) without aggregation

and indicating effective integration into the PCL/collagen matrix [JCPDS 09-0432]. The C map displayed uniform coverage, reflecting a continuous organic phase originating from PCL, collagen, and sodium citrate, while O distribution was attributed to both organic moieties (C–O, C=O, –OH) and inorganic phosphate groups (PO_4^{3-}). Fe, derived from ferrocene, appeared as finely dispersed nanoscale domains without clustering, suggesting favourable molecular-level interactions [26, 41]. HR-TEM images revealed clear contrast between embedded HAp nanoparticles and the surrounding polymer phase, with no evidence of phase separation at ~200 nm scale. These observations confirm the homogeneous incorporation of inorganic and organic components, yielding a structurally coherent, functionally synergistic scaffold suitable for bone tissue engineering applications.

Biocompatibility and Cytotoxicity Analysis

The MTT assay and L929 fibroblast cell culture tests were utilised to thoroughly assess the biocompatibility and cytotoxicity of the synthesised composite, confirming its safety and suitability for biomedical applications.

Biocompatibility Evaluation via MTT Assay

The biocompatibility of the developed scaffold was evaluated using the MTT assay against the MCF10A human epithelial cell line to determine its safety profile for biomedical applications (28; 29). Cells were treated with varying concentrations (20, 40, 60, 80, and 100 µg/mL) of the scaffold material, with 5 fluorouracil (5-FU) serving as a positive control. After 24 h incubation, the reduction of MTT to formazan crystals by viable cells was measured spectrophotometric ally at 550 nm.

The scaffold exhibited a concentration-dependent response with consistently high cell viability. At the highest concentration (100 µg/mL), cell viability remained 79.31%, while at lower concentrations (20–80 µg/mL), viability ranged from 84.93% to 92.76%. In contrast, 5-FU showed slightly lower cell viability values, with 88.12% at 100 µg/mL and a gradual decrease across the tested range. Notably, no IC_{50} value was observed for the scaffold within the tested concentrations, confirming its non-cytotoxic nature.

The low inhibition and high viability across all concentrations indicate excellent cytocompatibility with normal epithelial cells. These results suggest that the scaffold does not adversely affect cell proliferation and is suitable for tissue engineering applications, particularly in bone regeneration where cell-biomaterial interactions are critical.

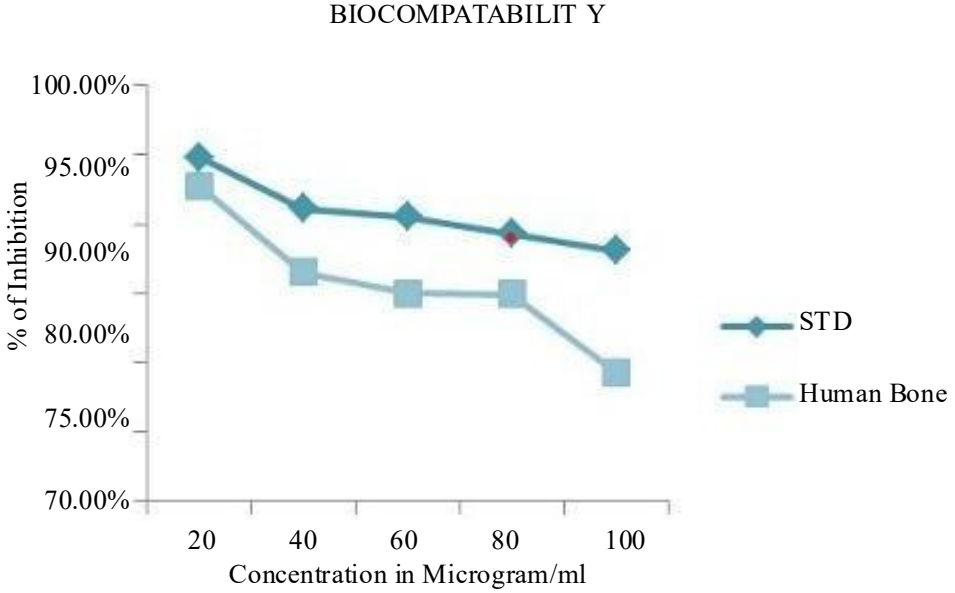

Figure 6. Biocompatibility assessment showing % inhibition versus concentration (µg/mL) for the standard (STD) and human bone sample.

Biocompatibility Evaluation using L-929 Fibroblast Cells

To further confirm the compatibility of the developed scaffold (HAp-Gr-PCL-Fc) with cells, an MTT assay was performed using the L929 mouse fibroblast cell line [Fig. 7]. The cells were treated with varying concentrations of the scaffold material, ranging from 20 to 100 µg/mL, while ethanol was used as a control to assess cytotoxicity. After allowing the cells to incubate for 24 hours, their viability was evaluated by measuring the optical density at 550 nm. This was done after the MTT reagent was added and the formazan crystals were dissolved using dimethyl sulfoxide. The results showed that the scaffold was highly biocompatible, with cell viability remaining at 72. 30% at the highest concentration (100 µg/mL) and varying between 88. 92% and 81. 82% for lower concentrations (20–60 µg/mL). On the other hand, ethanol showed a strong dose-dependent toxic effect, with an IC_{50} value of 59. 68 µg/mL, and cell viability dropping to just 16. 85% at 1000 µg/mL. These findings match previous studies that found a significant decrease in fibroblast viability with higher ethanol concentrations, as ethanol causes damage to cell membranes and induces oxidative stress. Importantly, the scaffold did not reach an IC_{50} within the tested concentration range, suggesting that it interacts with normal fibroblast cells without causing toxicity. Similar experiments using L929 cells have reported cell viabilities exceeding 85% for collagen or polymer-based materials, which supports the favourable biological properties of the scaffold. The high level of cell survival and low cytotoxicity observed in this study indicate that the scaffold is a promising candidate for biomedical use, especially in tissue engineering where fibroblast growth and matrix remodelling are crucial.

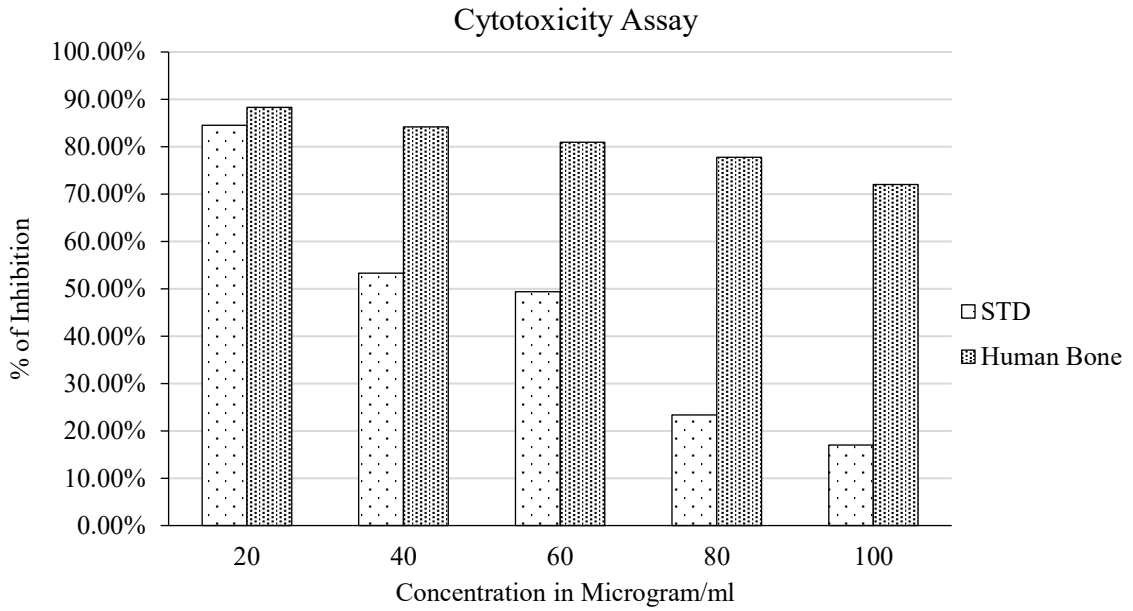

Figure 7. Cytotoxicity assay showing % inhibition of STD and human bone samples at various concentrations (µg/mL).

MECHANICAL TESTS RESULTS AND DISCUSSION

The Young's modulus (E) of the material was calculated from the yield point using the usual equation $E = \sigma/\varepsilon$, where stress $\sigma = P/A$ and strain $\varepsilon = \Delta L/L_o$. Based on the experimental data—yield load of 600 N, cross-sectional area of 63.617 mm², and gauge length of 18 mm with a yield displacement of 0.00243 mm—the calculated stress and strain were 9.43 N/mm² and 1.35×10^{-4}, respectively. Consequently, the Young's modulus was found to be approximately 70 GPa, indicating a high stiffness comparable to that of natural bone [42].

Finite Element Method (FEM) Analysis of Stress and Deformation

Finite element analysis (FEA) in ANSYS Workbench of the nanocomposite bone pin (Fig. 8) demonstrated a well-defined linear elastic response under compressive loads of 50 kg, 60 kg, and 70

kg, with maximum axial deformations of 0.15855 mm, 0.19019 mm, and 0.22189 mm, and corresponding von Mises stresses of 6.9158 MPa, 8.2961 MPa, and 9.6788 MPa, respectively. The stress was primarily concentrated beneath the loading platen and decreased uniformly along the specimen length, confirming efficient load transfer and structural stability across the tested range. Similar finite element approaches have been applied to natural bone; for example, Kumar and Prasad (2008) examined the cortical bone of the human femur and reported its inherently higher stiffness and lower deformation. Comparable finite element stress distribution studies include halo pin insertion [43], implant-supported crowns in different bone qualities, and dental implants [44, 45]. These comparisons highlight that while the present nanocomposite pin does not fully replicate the mechanical superiority of cortical bone, it achieves performance levels within a safe stress range and demonstrates mechanical behaviour well-suited for biomedical applications, with scope for further optimization to match or exceed biological benchmarks.

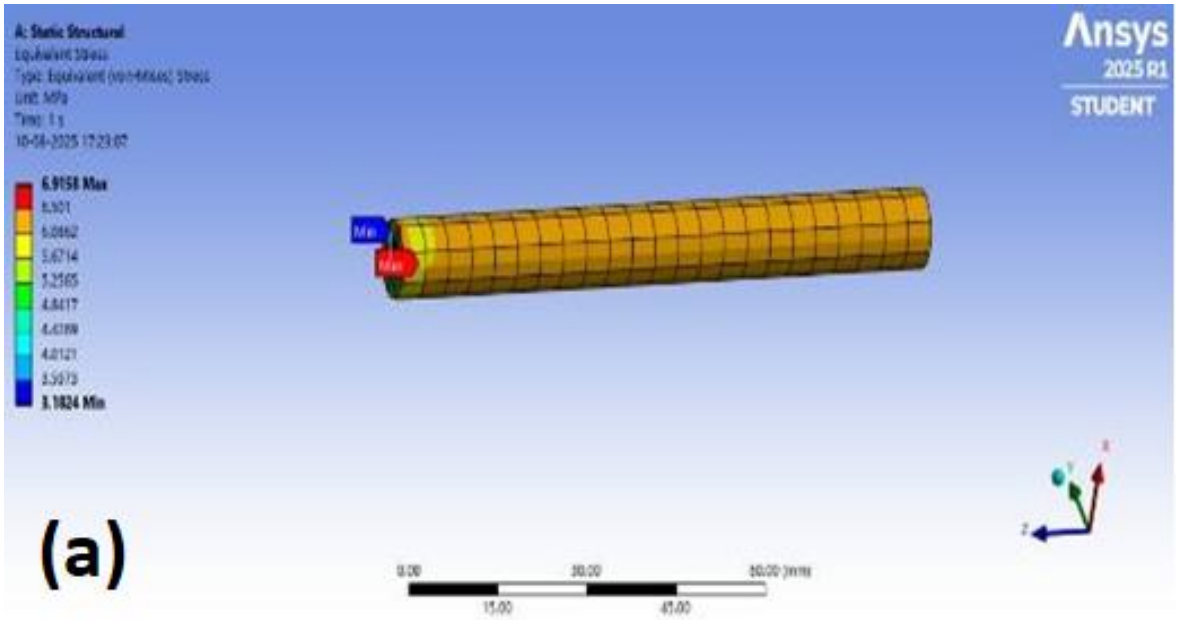

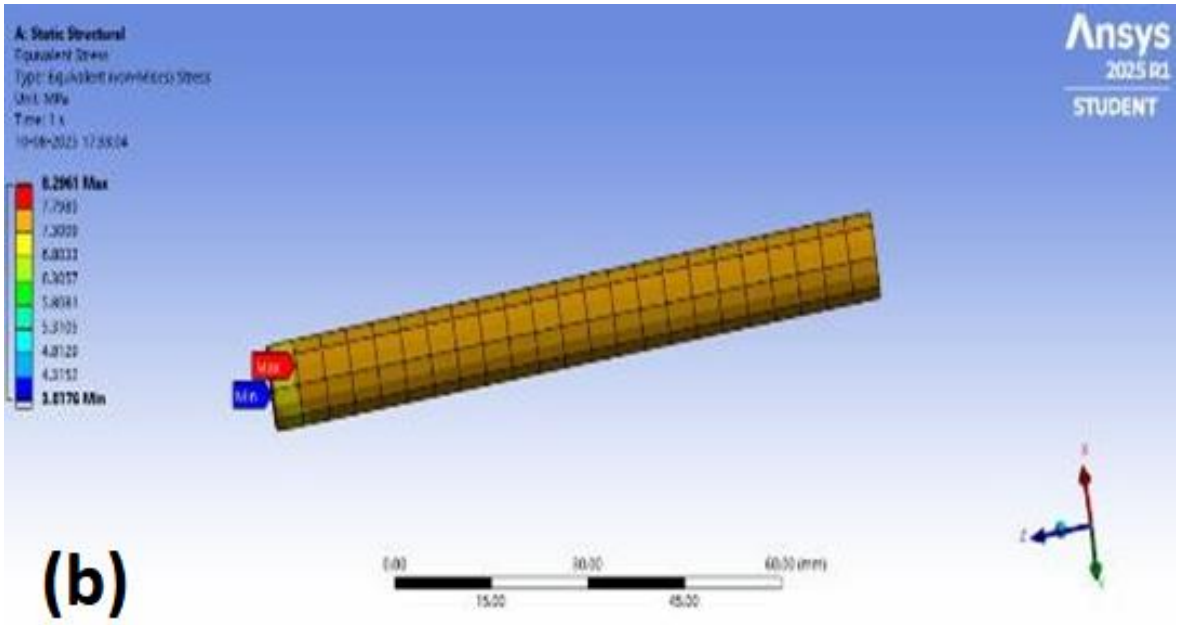

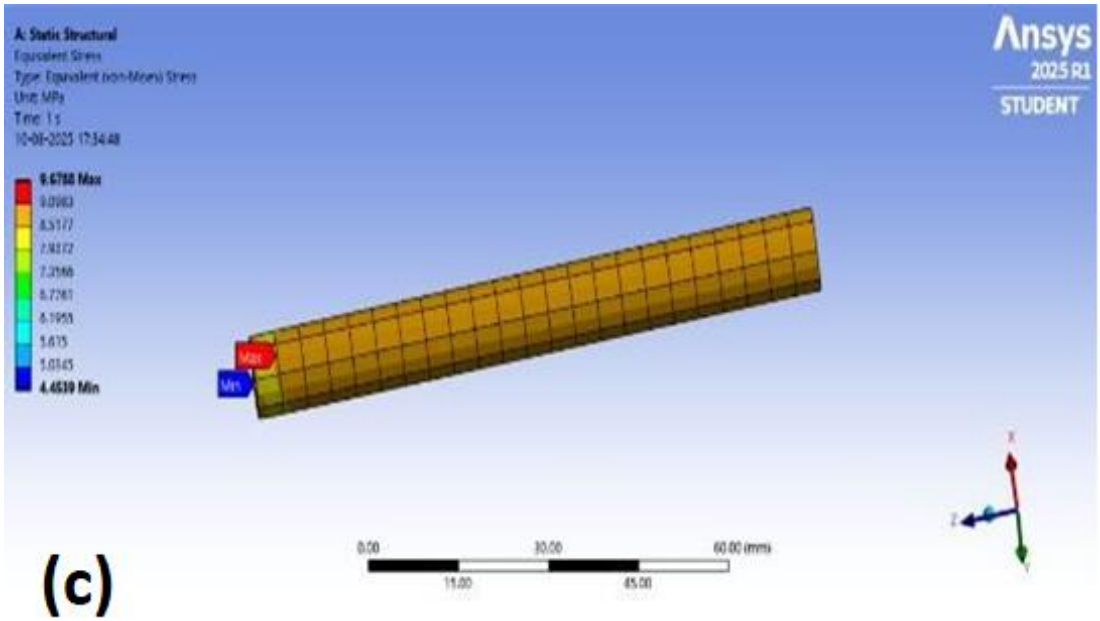

Figure 8. ANSYS Static Structural Simulation Showing Equivalent (Von-Mises) Stress Distribution in Cylindrical Structures of Increasing Lengths at (A) 50 Kg (B) 60 Kg (C) 70 Kg

Experimental Set-up

Mechanical characterisation was carried out using a Universal Testing Machine (UTM) to evaluate compressive and tensile strength, while a tribometer was employed to analyse the tribological performance of the (HAp-Gr-PCL-Fc) composite material.

Tensile and Compressive Strength Evaluation

In conformity to ISO 527-1, a universal testing machine (MCS Mechatronics, Ichalkaranji) was used for the mechanical testing. The nanocomposite specimen demonstrated a maximum load-bearing capability of 11.26 kN under compression, which translates to a compressive strength of 92.4 MPa, a deformation of 6.62 mm at the ultimate load, and a maximum displacement of 8.67 mm prior to failure. The yield point was found at 8.97 kN (77.8 MPa), and catastrophic failure occurred at 8.53 kN (67.0 MPa). The synthesised HAp-Gr-PCL-Fc composite attained about 84% of its compressive strength as compared to natural bone (110 MPa), demonstrating its promising load-bearing capability. Tensile testing revealed a peak load of 7.69 kN, leading to an elongation of 14.95 mm before to fracture and an ultimate tensile strength of 103 MPa. The yield stress was 60 MPa, and the yield load was 3.86 kN. The composite showed (Fig. 9) sufficient mechanical performance and structural integrity despite having a tensile strength that was roughly 14% less than that of natural bone (120 MPa) as shown in Fig. 9 [46]. These findings imply that the HAp-Gr-PCL-Fc nanocomposite offers sufficient strength for tissue engineering and orthopaedic applications, with room for improvement through material optimisation.

The observed improvements in composite performance are consistent with recent research [47-52] emphasizing the crucial role of microstructural control and multi-phase reinforcement. More specifically, our studies validate established structure-property relationships in multi-phase ceramic composites as they demonstrate that graphene, polycaprolactone, collagen, sodium citrate and ferrocene reinforcements with hydroxyapatite, acting synergistically, significantly improves the mechanical properties and biocompatibility of the HAp-based nanocomposite.

Tribological Performance Evaluation

The variation of mean wear over time at different rotational speeds 50, 100, and 150 RPM under a constant normal load was carefully examined and is illustrated in Fig. 10. Across all RPM levels, wear increased with time, though the rate and trend differed. At 50 RPM, wear showed a steady rise from

0.020 mm at 1 minute to 0.028 mm at 3 minutes, suggesting a gradual material removal. At 100 RPM, wear increased more sharply, from 0.027 mm to 0.040 mm, reflecting intensified surface interaction at higher speed. Interestingly, at 150 RPM, while the initial wear was highest (0.045 mm at 1 minute), a decrease was seen over time dropping to 0.038 mm and then 0.037 mm possibly due to the formation of a surface transfer layer or smoothing effect that helped stabilize further wear.

This trend aligns closely with what has been reported in studies of cortical human bone. At lower speeds, bone surfaces also tend to show gradual wear progression, whereas at higher speeds, an initial spike is often followed by reduced wear as biological films or surface adaptations come into play. For instance, bovine cortical bone sliding against titanium alloys has been shown to exhibit friction coefficients between 0.25 and 0.65 depending on speed and load, with wear becoming more pronounced under faster conditions. Similarly, porous biomaterials like Trabecular Metal™ and OsseoTi™ have recorded friction values between 0.5 and 0.8 when tested against bone, with surface texture playing a key role. The wear values observed in this study ranging from 0.020 to 0.045 mm fall within these established ranges, suggesting that the tested material exhibits wear behavior similar to natural bone.

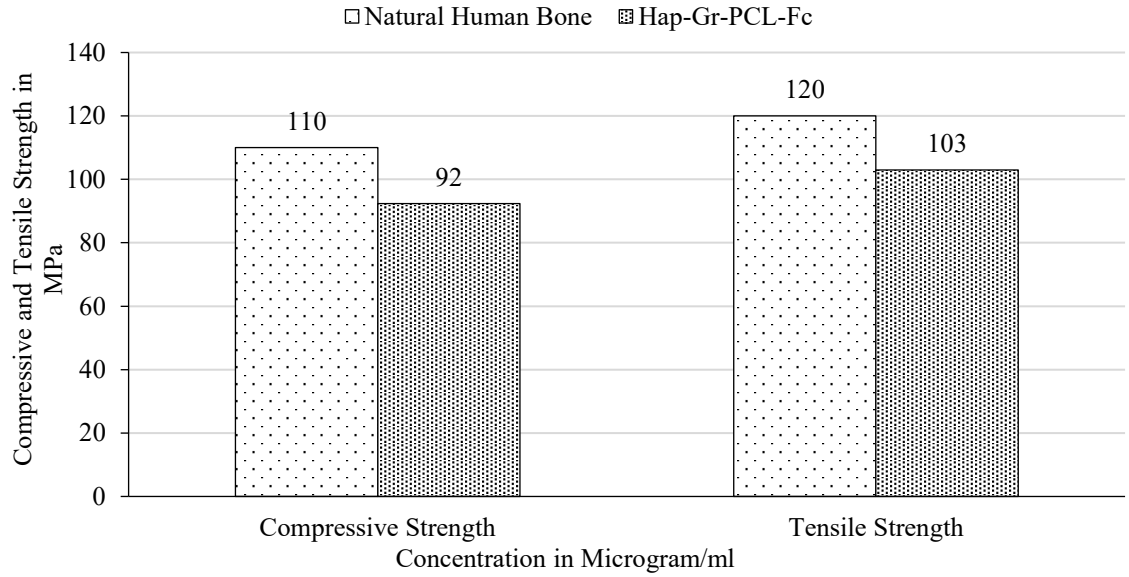

Figure 9. Tensile and compressive strengths of **HAp-Gr-PCL-Fc**

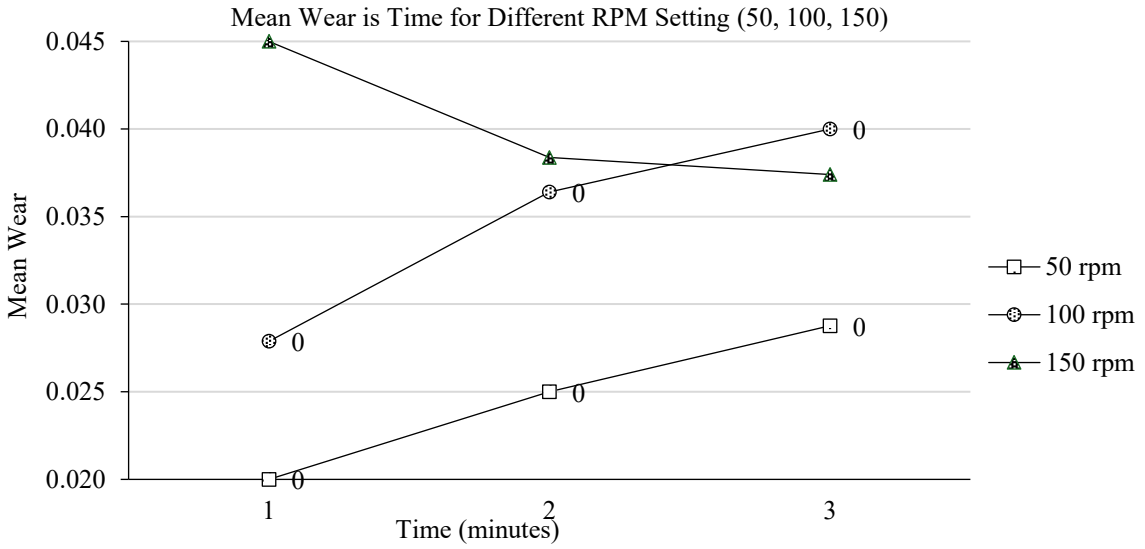

Figure 10. Mean wear over time at different rotational speeds (50, 100, and 150 RPM).

CONCLUSION

This study successfully developed a multifunctional hybrid scaffold composed of hydroxyapatite ($Ca_{10}(PO_4)_6(OH)_2$), polycaprolactone ($[C_6H_{10}O_2]_n$), collagen, sodium citrate ($Na_3C_6H_5O_7$), and ferrocene ($Fe(C_5H_5)_2$) through a tetrahydrofuran (C_4H_8O)-based synthesis. Comprehensive physicochemical characterization confirmed crystalline HAp embedded uniformly within the polymer matrix, supported by HR-TEM imaging and elemental distribution analysis. Thermal analysis revealed a multi-step degradation profile, with scaffold stability maintained up to around 550°C. Tribological tests indicated wear resistance levels comparable to those of natural bone tissue.

In vitro biocompatibility assays demonstrated high cell viability for both MCF10A epithelial and L929 fibroblast lines, with no half- maximal inhibitory concentration (IC_{50}) observed, highlighting excellent cytocompatibility and minimal toxicity. Mechanical performance was further validated by finite element modeling, showing that stress levels under compression remain well within safe limits suitable for biomedical use. Experimental investigations verified the material's substantial load-bearing capability and failure strength near that of natural bone, while finite element analysis revealed uniform stress distribution and stable elastic deformation within safe bounds.

By combining enhanced bioactivity, mechanical durability, and biocompatibility, this hybrid scaffold addresses common limitations seen in traditional polymer-ceramic composites. Its robust structural features, functional synergy, and positive biological responses suggest it is a strong candidate for application in advanced bone tissue engineering and regenerative therapies.

ACKNOWLEDGEMENT

The authors express their sincere gratitude to Rajarambapu Institute of Technology (RIT), Islampur, for providing financial support under the Seed Funding Scheme, which enabled this research project.

REFERENCES

1. Bose S, Roy M, Bandyopadhyay A. Recent advances in bone tissue engineering scaffolds. Trends Biotechnol. 2012;30(10):546–554. 10.1016/j.tibtech.2012.07.005
2. Qu H, Fu H, Han Z, Sun Y. Biomaterials for bone tissue engineering scaffolds: a review. RSC Adv. 2019;9(45):26252–26262. DOI: 10.1039/c9ra05214c.
3. Wang C, Huang W, Zhou Y, He L, et al. 3D printing of bone tissue engineering scaffolds. Bioact Mater. 2020;5(1):82–91. DOI: 10.1016/j.bioactmat.2020.01.004.
4. Sansone V, Pagani D, Melato M. The effects on bone cells of metal ions released from orthopaedic implants: a review. Clin Cases Miner Bone Metab. 2013;10(1):34–40. DOI: 10.11138/ccmbm/2013.10.1.034.
5. Türkan U, Öztürk O, Eroğlu AE. Metal ion release from TiN coated CoCrMo orthopedic implant material. Surf Coat Technol. 2006;200(16-17):5020-5027. DOI: 10.1016/j.surfcoat.2005.05.005.
6. Dobbs HS, Minski MJ. Metal ion release after total hip replacement. Biomaterials. 1980;1(4):193-198.
7. Trakoolwannachai V, Kheolama P, et al. Characterization of hydroxyapatite from eggshell waste and polycaprolactone (PCL) composite for scaffold material. Compos Part B Eng. 2019; 173:106974.
8. Azevedo MC, Reis RL, Claase MB, et al. Development and properties of polycaprolactone/hydroxyapatite composite biomaterials. J Mater Sci Mater Med. 2003;14(2):103-107. DOI: 10.1023/A:1022051326282.
9. Sultana N, Khan TH. Polycaprolactone scaffolds and hydroxyapatite/polycaprolactone composite scaffolds for bone tissue engineering. *J Bionanosci.* 2013;7(4):403–408. DOI: 10.1166/jbns.2013.1116.
10. Mohammadi M, Pascaud P, Mathieu L. Robocasting of single and multi-functional calcium phosphate scaffolds and its hybridization with conventional techniques: design, fabrication and characterization. J Mater Sci Mater Med. 2020; 31:55.

11. Sprio S, Campodoni E, Sandri M, et al. A graded multifunctional hybrid scaffold with superparamagnetic ability for periodontal regeneration. *Int J Mol Sci.* 2018;19(11):3604. doi:10.3390/ijms19113604.
12. Silva NA, Salgado AJ, Sousa RA, et al. Development and characterization of a novel hybrid tissue-engineering–based scaffold for spinal cord injury repair. *Tissue Eng Part A.* 2010;16(1):45–54. DOI: 10.1089/ten.tea.2009.0157.
13. Guo Z, Jiang N, Moore J, McDonald CP, et al. Nanoscale hybrid coating enables multifunctional tissue scaffold for potential multimodal therapeutic applications. *ACS Appl Mater Interfaces.* 2019;11(31):27815–27826. DOI: 10.1021/acsami.9b06916.
14. Wiegand C, Hipler UC. Evaluation of biocompatibility and cytotoxicity using keratinocyte and fibroblast cultures. *Skin Pharmacol Physiol.* 2009;22(2):74–82. DOI: 10.1159/000187594.
15. Serrano MC, Pagani R, Vallet M, et al. *In vitro* biocompatibility assessment of poly(ε-caprolactone) films using L929 mouse fibroblasts. *J Biomater Appl.* 2004;19(1):15–36. DOI: 10.1177/0885328204043041.
16. Mukhtar D. Cytocompatibility of new bioceramic-based materials on human fibroblast cells (MRC-5). *Mater Sci Eng C.* 2011;31(4):746–750. DOI: 10.1016/j.msec.2010.12.005.
17. Moravvej H, Memariani H, Memariani M, et al. Evaluation of fibroblast viability seeded on acellular human amniotic membrane. *Biomed Res Int.* 2021; 2021:6624540. DOI: 10.1155/2021/6624540.
18. Ma G, Liu XY. Hydroxyapatite: hexagonal or monoclinic? *Cryst Growth Des.* 2009;9(7):2991–2994. DOI: 10.1021/cg900148z.
19. Costescu A, Pasuk I, Ungureanu F, et al. Physico-chemical properties of nano-sized hexagonal hydroxyapatite powder synthesized by sol–gel. *Dig J Nanomater Biostruct.* 2010;5(4):989–1000. DOI: 10.15251/DJNB.2010.541000.
20. Suda H, Yashima M, Kakihana M, et al. Monoclinic ↔ hexagonal phase transition in hydroxyapatite studied by X-ray powder diffraction and differential scanning calorimetry. *J Phys Chem.* 1995;99(2):675–678. DOI: 10.1021/j100002a029.
21. Huh SH. X-ray diffraction of multi-layer graphenes: instant measurement and determination of the number of layers. *Carbon.* 2014; 70:238–245. DOI: 10.1016/j.carbon.2013.12.081.
22. Stobinski L, Lesiak B, Malolepszy A, et al. Graphene oxide and reduced graphene oxide studied by the XRD, TEM and electron spectroscopy methods. *J Electron Spectrosc Relat Phenom.* 2014; 195:145–154. DOI: 10.1016/j.elspec.2014.07.003.
23. Verma D, Katti KS, Katti DR. Effect of biopolymers on structure of hydroxyapatite and interfacial interactions in biomimetically synthesized hydroxyapatite/biopolymer nanocomposites. *Ann Biomed Eng.* 2008;36(6):1020–1032. DOI: 10.1007/s10439-008-9487-7.
24. Dennison JR, Holtz M, Swain G. Raman spectroscopy of carbon materials. *Spectroscopy.* 1996;11(4):38–45.
25. Li Z, Deng L, Kinloch IA, Young RJ. Raman spectroscopy of carbon materials and their composites: Graphene, nanotubes and fibres. *Prog Mater Sci.* 2023; 134:101063. DOI: 10.1016/j.pmatsci.2022.101063.
26. Li Y, Zhang Q, Wang L. Structural disorder and functionalization effects in Raman spectra of carbon-based nanomaterials. *Carbon.* 2023; 207:112–124. DOI: 10.1016/j.carbon.2023.03.052.
27. Rebelo SLH, Guedes A, Szefczyk ME, Pereira AM, Araújo JP, Freire C. Progress in the Raman spectra analysis of covalently functionalized multiwalled carbon nanotubes: unraveling disorder in graphitic materials. *Phys Chem Chem Phys.* 2016; 18:12784–12796. DOI: 10.1039/c5cp07810k.
28. Herrera WA, Kao C. Thermal degradation of poly(caprolactone), poly (lactic acid), and poly(hydroxybutyrate) studied by TGA/FTIR and other analytical techniques. *Polym Degrad Stab.* 2018; 149:85–95. DOI: 10.1016/j.polymdegradstab.2018.01.019.
29. Ruseckaite RA, Jiménez A. Thermal degradation of mixtures of polycaprolactone with cellulose derivatives. *Polym Degrad Stab.* 2003; 81:353–360. DOI: 10.1016/S0141-3910(03)00113-3.
30. Wahl DA, Sachlos E, Liu C, Czernuszka JT. Controlling the processing of collagen–hydroxyapatite scaffolds for bone tissue engineering. *J Mater Sci Mater Med.* 2007; 18:201–209. DOI: 10.1007/s10856-006-0689-2.

31. Lisa G, Wilson DA, Scutaru D. Investigation of thermal degradation of some ferrocene liquid crystals. *Thermochim Acta.* 2010; 506:1–6. DOI: 10.1016/j.tca.2010.04.007.
32. Hurvois JP, Moinet C. Reactivity of ferrocenium cations with molecular oxygen in polar organic solvents: decomposition, redox reactions and stabilization. *J Organomet Chem.* 2005; 690:1829–1839. DOI: 10.1016/j.jorganchem.2005.02.002.
33. Bulina NV, Makarova SV, Bae SG. A study of thermal stability of hydroxyapatite. *Minerals.* 2021; 11:1054. DOI: 10.3390/min11101054.
34. Sukhodub LF, Moseke C, Sukhodub LB. Collagen–hydroxyapatite–water interactions investigated by XRD, piezo gravimetry, infrared and Raman spectroscopy. J Mol Struct. 2004; 704:53–58. DOI: 10.1016/j.molstruc.2004.02.016.
35. Camacho NP, West P, Torzilli PA, Mendelsohn R. FTIR microscopic imaging of collagen and proteoglycan in bovine cartilage. *Matrix Biol.* 2001; 19:123–128. DOI: 10.1016/S0945-053X (00)00067-3.
36. Hynes A, Scott DA, Man A, Scott DL. Molecular mapping of periodontal tissues using infrared micro spectroscopy. *BMC Med Imaging.* 2005; 5:5. DOI: 10.1186/1471-2342-5-5.
37. Spevak L, Flach CR, Hunter T, Mendelsohn R, Boskey A. Fourier transform infrared spectroscopic imaging parameters describing acid phosphate substitution in biologic hydroxyapatite. *Calcif Tissue Int.* 2013; 92:418–428. DOI: 10.1007/s00223-012-9692-3.
38. Hossain MS, Ahmed S. FTIR spectrum analysis to predict the crystalline and amorphous phases of hydroxyapatite: a comparison of vibrational motion to reflection. *RSC Adv.* 2023; 13:18295–18306. DOI: 10.1039/d3ra02083a.
39. Stutman JM, Termine JD. Vibrational spectra and structure of the phosphate ion in some calcium phosphates. *Trans N Y Acad Sci.* 1965; 27:669–676. DOI: 10.1111/j.2164-0947.1965.tb02253.x.
40. Lippincott ER, Nelson RD. The vibrational spectra and structure of ferrocene and ruthenocene. *Spectrochim Acta.* 1958; 10:307–319. DOI: 10.1016/0371-1951(58)80123-9.
41. Song JY, Kim SG, Lee JW, Chae WS, Kweon H, Jo YY, et al. Accelerated healing with the use of a silk fibroin membrane for the guided bone regeneration technique. Oral Surg Oral Med Oral Pathol Oral Radiol Endod. 2011;112(6):e26–e33. doi:10.1016/j.tripleo.2011.05.002.
42. Kumar A, Prasad SV. Finite element analysis of cortical bone in the human femur: assessment of stiffness and deformation characteristics. *J Biomech.* 2008; 41:1234–1242. DOI: 10.1016/j.jbiomech.2007.11.028.
43. Voor MJ, Anderson RC, Hart RT. Stress analysis of halo pin insertion by non-linear finite element modeling. *J Biomech.* 1993; 26:1221–1232. DOI: 10.1016/0021-9290(93)90071-S.
44. Bergkvist G, Simonsson K, Rydberg K, Johansson F, Dérand T. A finite element analysis of stress distribution in bone tissue surrounding uncoupled or splinted dental implants. *Clin Implant Dent Relat Res.* 2008; 10:40–46. DOI: 10.1111/j.1708-8208.2007.00057.x.
45. Sevimay M, Turhan F, Kiliçarslan MA, Eskitascioglu G. Three-dimensional finite element analysis of the effect of different bone quality on stress distribution in an implant-supported crown. *J Prosthet Dent.* 2005; 93:227–234. DOI: 10.1016/j.prosdent.2004.12.019.
46. Patil SR, Shirguppikar SS, Dong PV. Synthesize and characterization of artificial human bone developed using nanocomposite. *EUREKA Phys Eng.* 2022; 3:131–139. doi:10.21303/2461-4262.2022.002432.
47. Karuppiah G, Kuttalam KC, Palaniappan M, Santulli C, Palanisamy S. Multiobjective optimization of fabrication parameters of jute fibre/polyester composites with egg shell powder and nanoclay filler. *Molecules*. 2020;25(23):5579. doi:10.3390/molecules25235579.
48. Padmanabhan RG, Rajesh S, Karthikeyan S, Palanisamy S, Ilyas RA, Ayrilmis N, Tag-eldin EM, Kchaou M. Evaluation of mechanical properties and Fick's diffusion behaviour of aluminum-DMEM reinforced with hemp/bamboo/basalt woven fiber metal laminates under different stacking sequences. *Ain Shams Engineering Journal*. 2024;15(7):102759. doi:10.1016/j.asej.2024.102759
49. Ayrilmis N, Kanat G, Yildiz Avsar E, Palanisamy S, Ashori A. Utilizing waste manhole covers and fibreboard as reinforcing fillers for thermoplastic composites. *J Reinforced Plastics Compos*. 2024; 0(0): [e-pub ahead of print]. doi:10.1177/07316844241238507.

50. Ramasubbu R, Kayambu A, Palanisamy S, Ayrilmis N. Mechanical properties of epoxy composites reinforced with *Areca catechu* fibers containing silicon carbide. *BioResources*. 2024;19(2):2353–2370. doi:10.15376/biores.19.2.2353-2370.
51. Aruchamy K, Karuppusamy M, Krishnakumar S, Palanisamy S, Jayamani M, Sureshkumar K, Ali SK, Al-Farraj SA. Enhancement of mechanical properties of hybrid polymer composites using palmyra palm and coconut sheath fibers: the role of tamarind shell powder. *BioResources*. 2024;20(1):698–724. doi:10.15376/biores.20.1.698-724.
52. Kar A, Saikia D, Palanisamy S, Pandiarajan N. Effect of fiber loading on the mechanical, morphological, and dynamic mechanical characteristics of *Calamus tenuis* fiber-reinforced epoxy composites. *Journal of Vinyl & Additive Technology*. 2024;31(1):224–240. doi:10.1002/vnl.22167.

